New Journal of Physics
The open access journal at the forefront of physics

Deutsche Physikalische Gesellschaft DPG
IOP Institute of Physics

Published in partnership with: Deutsche Physikalische Gesellschaft and the Institute of Physics

OPEN ACCESS

RECEIVED
5 October 2014

REVISED
13 February 2015

ACCEPTED FOR PUBLICATION
17 March 2015

PUBLISHED
17 April 2015

PAPER

Superconductivity in an expanded phase of ZnO: an *ab initio* study

D Hapiuk[1], M A L Marques[1], P Mélinon[1], S Botti[1], B Masenelli[2] and J A Flores-Livas[3]

[1] Université de Lyon, F-69000, France; Univ. Lyon 1, Institut Lumière Matière; CNRS, UMR 5586; F69622 Villeurbanne Cedex
[2] Université de Lyon, F-69000, France; Institut des Nanotechnologies de Lyon; UMR 5270 CNRS and INSA Lyon, 7 avenue Jean Capelle, 69621 Villeurbanne CEDEX, France
[3] Max-Planck Institut für Mikrostrukturphysik, Weinberg 2, D-06120 Halle, Germany

E-mail: dimitri.hapiuk@gmail.com **and** patrice.melinon@univ-lyon1.fr

Keywords: ZnO, sodalite, superconductivity, doping, ionic, *ab initio*

Supplementary material for this article is available online

Abstract

It is known that covalent semiconductors become superconducting if conveniently doped with large concentration of impurities. In this article we investigate, using *ab initio* methods, if the same situation is possible for an ionic, large-band gap semiconductor such as ZnO. We concentrate on the cage-like sodalite phase, with very similar electronic and phononic properties as wurtzite ZnO, but allow for endohedral doping of the cages. We find that sodalite ZnO becomes superconducting for a variety of dopants, reaching a maximum critical temperature of 7 K. This value is comparable to the transition temperatures of doped silicon clathrates, cubic silicon, and diamond.

1. Introduction

Conventional superconductivity is a relatively common property of metals at low temperature. However, approximately a decade ago, the scientific community was taken by surprise when also simple semiconductors, if properly doped, were found to superconduct. The original discovery was boron-doped diamond in 2004 [1], but silicon (doped with boron [2]), germanium (doped with gallium [3]), and silicon carbide (doped with boron [4] or aluminum [5]) soon followed. These materials are members of a more exclusive group that is characterized by covalent bonds instead of the typical metallic bonding of traditional superconductors [6]. Other members of this group include the high-temperature copper oxide ceramics [7], MgB_2 [8, 9], the alkali-doped fullerenes [10], disilicides [11, 12], and intercalated graphites [13, 14]. It is now generally accepted that (perhaps many) covalent semiconductors can be transformed into conventional superconductors if an appropriate doping strategy can be found. However, what is still not clear is if ionic semiconductors can also become superconducting. The bonding character of an ionic material is certainly very different from a covalent or metallic system, with the electrons localized around the atoms and strong internal electric fields. In this article we show, using *ab initio* methods, how this physical situation can also lead to superconductivity.

We decided to choose ZnO as a test case, as it is certainly one of the most studied ionic semiconductors. It has a relatively large gap (3.4 eV) and high excitonic binding energy (60 meV). Moreover, it is actually a cheap and eco-friendly potential alternative to GaN, widely used in industry. This makes ZnO an excellent candidate for opto-electronic applications, such as the fabrication of transparent electrodes [15] and white diodes [16]. Besides it could be used in nanoelectronics via bottom-up strategies [17, 18]. ZnO in the usual wurzite phase can be readily doped with electrons, but p-doping remains elusive. This behavior arises from a variety of causes, including native crystalline defects and impurity incorporations [19]. In any case, the dopant levels that can nowadays be reached experimentally are certainly too low for superconductivity.

To circumvent this problem, we will take a lesson from history. In 2003 it was found that an expanded, cage-like allotrope of silicon could become superconducting. In this so-called clathrate structure silicon atoms shared the tetrahedral coordination of cubic silicon, but the large empty space inside the cages allowed for endohedral doping. Endohedral doping might not be as efficient as substitutional doping to give or remove electrons from the lattice, but it certainly makes it much easier to reach doping concentrations of several percent. Moreover,

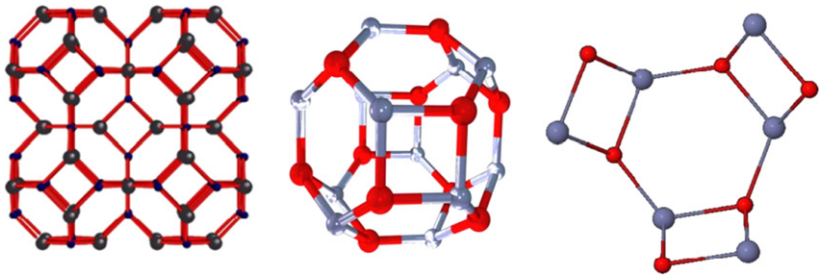

Figure 1. Representation of the sodalite (left), of one of its elementary cages (middle), and its unit cell (right).

lattice deformations are less pronounced than in the case of substitutional doping. Endohedral doping of silicon clathrates by alkaline atoms allows the control of the electronic properties up to the appearance of superconductivity. The critical temperature was predicted to reach 8 K for a heavy dopant like barium, in agreement with experimental studies [20, 21]. To a large extent it was the study of these silicon clathrates that led to the subsequent discovery of superconductivity in standard group-IV semiconductors [22].

We will take a similar path, and look at expanded phases of ZnO. There is a very rich literature on these phases, and many different zeolite structures have been studied. Our choice falls on the sodalite, the simplest and most symmetric metastable ZnO cage-like structure (SOD, according to the nomenclature of the International Zeolite Association) [23–27]. It consists of a regular stacking with *Pm3n* symmetry of truncated octahedra, which are Archimedean solids with 14 faces (eight regular hexagons and six squares), leading to the net formula $(ZnO)_{12}$ (see figure 1). It is also the original solution to Kelvin's problem (space-filling polyhedra with cells being separated by walls of minimal total area). Although, there is no known pathway to synthesize ZnO sodalite yet, the existence of its building blocks has already already proven experimentally. Theoretical [28–30] and experimental studies [31] agree that the $(ZnO)_{12}$ cluster is stable and energetically favored. Furthermore, very recent works point to the existence of ZnO cage-like nanostructures using photoelectron spectroscopy together with DFT calculations [32]. The $(ZnO)_{12}$ clusters identified in [32] are very similar to the building blocks of the sodalite structure. Finally, another experimental paper shows the existence of fullerene-like structures of ZnO produced by laser ablation and studied by time of flight mass spectroscopy [33]. Moreover, sodalite turns out to be a low-energy metastable structure for the family of III-V semiconductors [34]. In view of that, the sodalite structure is at present the most promising metastable cage-like phase of ZnO. However, other cage-like allotropes are under study. For instance, calculations have shown that the body-centered tetragonal (BCT) structure is more stable than the sodalite structure, with a cohesive energy very close to the wurtzite one (+0.030 meV/ZnO) [35]. Note that the BCT phase of ZnO has already been identified experimentally [36, 37]. However, although also the BCT phase is a cage-like structure, the volume of its unit cell is small and comparable to the one of wurtzite [35]. As a consequence, heavy endohedral doping is expected to be difficult. Of course, the study of endohedral doping and superconductivity in other cage-like structures of ZnO is certainly worthy, but this is beyond the scope of this manuscript, which focuses on one single low-energy high-volume phase, opening new perspectives for other cage-like structures.

Achieving p-type doping in ZnO is a long-standing problem [38]. Indeed, many attempts have been made to p-dope wurtzite ZnO samples without any real success. Cage-like structures are particularly suited for heavy endohedral doping due to their open geometry. This is experimentally proven for other compounds, such as Si clathrates [39]. In a previous work [35], we predicted that stable p-doping could be achieved in sodalite ZnO. Doped structures turned out to be even more stable than the undoped ones for some impurities. This is promising for the synthesis of doped sodalite around native dopants, analogous to what is already done for silicon, germanium, or tin clathrates [39]. Indeed, silicon clathrates are generally synthesized in two steps [40]: the synthesis of the precursor (silicide MSi, M being an alkaline element) followed by its pyrolysis. The silicides are prepared by treating stoichiometric mixtures of both elements Si and M with an arc-melting technique. Clathrate II is then obtained by heating the silicide under vacuum leading to the net formula $M_x@Si_{34}$ with x down to one [41, 42]. A similar synthesis route could potentially lead to cage-like structures for ZnO. Another possible synthesis route that could be explored is whether ZnO cage-like networks can be obtained starting from ZnO metal-oxide frameworks. The metal-oxide framework is already a cage-like structure, but it includes carbon chains. In this case, one needs to find a strategy to remove the carbon chains and replace them with inorganic ZnO units.

Sodalite ZnO remains a iono-covalent material with a ionicity very close to the one of the wurtzite structure (the Philipps ionicity of wurtzite ZnO is close to 0.616 [43]). Also the direct bandgap of sodalite ZnO is close to

Table 1. Features of the undoped and doped sodalite ZnO. For each element the dopant concentration, the space group of the structure after relaxation, the dynamical stability (absence of imaginary phonon frequencies) and the electronic DOS at the Fermi level $N(E_F)$ in eV^{-1} are reported.

	Concentration	Spacegroup	Stability	Doping	$N(E_F)$
Undoped	—	$Pm\bar{3}n$	Yes	—	0
Te	8%/14%	$Pm\bar{3}$/ $Pm\bar{3}n$	Yes	P-doped	3.3/7.4
Br	8%/14%	$Pm\bar{3}$/ $Pm\bar{3}n$	Yes	P-doped	10.1/19
Cl	8%/14%	$Pm\bar{3}$/ $Pm\bar{3}n$	Yes	P-doped	10.6/15.8
I	8%/14%	$Pm\bar{3}$/ $Pm\bar{3}n$	Yes	P-doped	3.0/10.9
In	14%	$Pm\bar{3}n$	Yes	N-doped	2.9
F	8%	$R3$	Yes	P-doped	9.3
Sb	8%/14%	$Pm\bar{3}$/ $Pm\bar{3}n$	No	P-doped	—
Sn	14%	$R3c$	No	P-doped	—
As, B, C	8%/14%	$R3$/ $R3c$	No	N-doped	—
Sr, Ba, Bi	14%	—	No	N-doped	—
Li, Na, Al	8%/14%	$Pm\bar{3}$/ $Pm\bar{3}n$	No	N-doped	—

the one of wurtzite ZnO [35]. This can be explained by the similar sp^3 bonding and bonding distance of the wurtzite and sodalite phases.

2. Methods

Our study starts with density-functional theory (DFT) calculations using the code ABINIT [44, 45]. The exchange-correlation functional was modeled by a Perdew, Burke, and Erzernhof (PBE) generalized gradient approximation [46] (GGA), while the electron–ion interaction was described by norm-conserving Troullier–Martins pseudopotentials generated with the same functional [47]. A proper convergence was ensured using a cutoff energy of 60 Ha and a $4 \times 4 \times 4$ Monkhorst–Pack k-mesh [48] for sampling the Brillouin zone. Unit cells (figure 1) were constituted of six Zn atoms, six O atoms and one or two dopant atoms building a cage-like material with one out of two cages filled (8% doping) or all cages filled (14% doping), respectively.

The phonon modes and the electron–phonon coupling matrix elements were then obtained within the framework of density-functional perturbation theory [49–51]. A $4 \times 4 \times 4$ grid of $\mathbf{q}$-wavevectors and the tetrahedron technique were used for the integration over the Fermi surface. We evaluated the superconducting transition temperatures using the well-known McMillan's formula [52, 53].

3. Results and discussions

We doped ZnO with a large number of different elements (see table 1) and two high doping concentrations (8% and 14%) were tested to ensure that the doped sodalite was a degenerate semiconductor. These concentrations correspond, respectively, to the case where every other cage is filled and where all cages are filled. Figure 2 illustrates the electronic density of states (DOS) and the geometry of doped structures for selected dopants and concentrations.

3.1. Geometric deformations

We first discuss the geometric consequences of high doping in sodalite ZnO. Panels (b) and (d) in figure 2 illustrate the two possible cases that appear when structures are relaxed. If the atomic radius of the dopant is small (e.g., F in panel (d) of figure 2), its equilibrium position is shifted by around 0.8 Å from the center of the cage. This is due to a Jahn–Teller effect, typical of cage-like structures such as silicon clathrates [21]. Furthermore, the deformation of the cage is strong and anisotropic. The inspection of the lattice distortions reveals repulsion between O and dopant atoms, while Zn atoms basically remain at their initial positions [35]. These deformations point to a strong hybridization between the electrons of the dopant and the ones of ZnO. On the contrary, if the atomic radius of the dopant is large (e.g., Te in panel (b) of figure 2), the dopant remains located at the center of the cage, inducing an isotropic deformation of the latter. The steric hindrance prevents any Jahn–Teller effect and any strong anisotropic deformation. The space groups of the different doped structures are summarized in table 1.

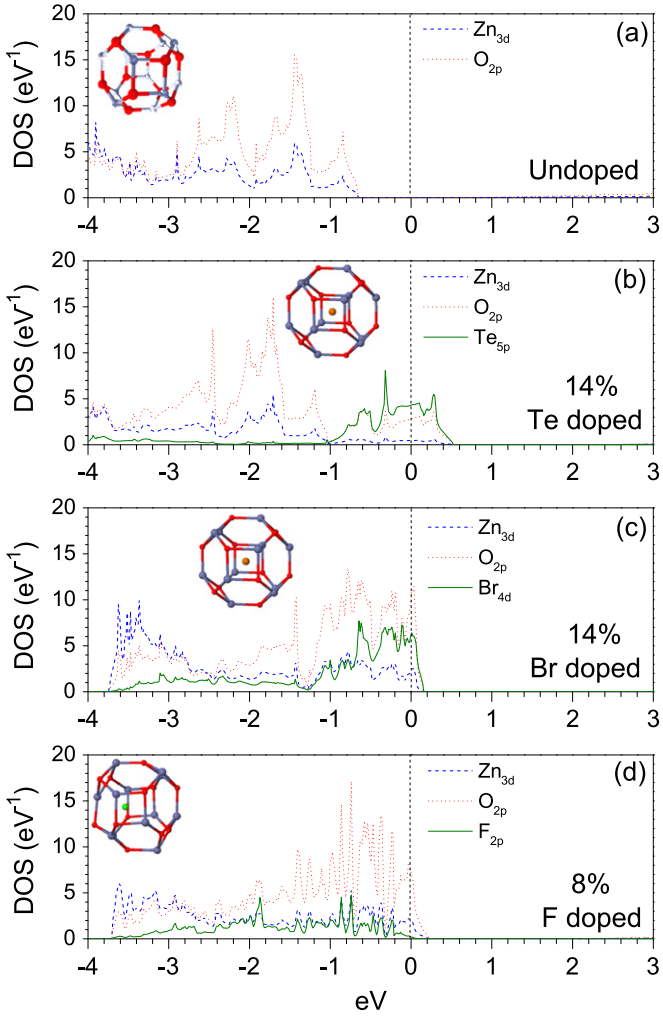

Figure 2. Atomic projected electronic DOS of undoped sodalite ZnO, and Te-, Br, and F-doped sodalite ZnO. The Fermi level is located at 0 eV. The doping concentration is near 14% for Te and Br and close to 8% for F. Each inset represents an elementary cage of the undoped or doped sodalite ZnO.

3.2. Electronics densities of states

To investigate the consequences of high-doping levels in the electronic structure, we show in figure 2 the projected electronic DOS of sodalite ZnO for some selected impurities that lead to stable doping. We note that the diffusion of dopants is sometimes possible in the lattice, leading to dimerization of the impurities and destroying the effect of doping [35]. For instance, this is the case for P, N, S, and Se. Furthermore, some doped structures do no exhibit dimerization but they are dynamically unstable, given the appearance of imaginary phonon frequencies (see table 1).

In figure 2 we see that the Fermi level (at 0 eV) is located inside the valence band for Te, F, and Br. These materials are thus p-type degenerate semiconductors. This feature is observed at both doping concentrations (8% and 14%). Among all elements tested, O, F, Cl, Br, I, and Te led to a stable p-type doping, whereas In gave a stable n-type doping. Moreover, doped structures exhibit quite high electronic DOS at the Fermi energy $N(E_F)$ (see table 1). This is an important point since, as discussed next, $N(E_F)$ is a limiting parameter for superconductivity in 3D structures (unlike 2D structures) [54]. The conclusion of this analysis is that, at high doping concentrations, endohedral doping in sodalite ZnO can be very efficient.

The examination of the atomic projection of the DOS reveals that the states contributing to the DOS at the Fermi level have mainly Zn_{3d}, O_{2p}, and X_p (where X is the dopant) character. Their relative contributions can be quite different, leading to three distinct scenarios. In the first one, the states at E_F are essentially hybridized X_p and O_{2p} states. Te- and I-doped sodalite belong to this group. In the case of Br- and Cl-doped sodalite Zn states have a stronger weight at E_F at the expense of the dopant states, which maintain a significantly larger weight than Zn states anyway. Finally, F- and In- doped sodalite constitute the third group, where the contribution of the dopant states to the DOS at E_F is negligible.

Note that the ZnO band gap is underestimated as expected, since we used a standard DFT functional. However, the superconducting properties are dependent on the DOS at E_F, situated inside the valence band of p-doped sodalite, which is accurately described by standard DFT functionals. We checked that the electronic structure near the Fermi level using different standard functionals and hybrid HSE06 exchange-correlation functional remains essentially unchanged.

3.3. Phonon densities of states

Aiming at evaluating the superconducting transition temperature, we performed calculations to obtain phonon band structures. Results are presented in figure 3 for undoped sodalite ZnO (panel (a)), for sodalite doped at 14% with Te (panel (b)) and Br (panel (c)), and at 8% for F (panel (d)). Phonon frequencies of pure sodalite range from 0 to 610 cm^{-1} with a gap at around 325 cm^{-1}. This gap is similar to the gap of wurtzite ZnO and it is due to the ionic-like character of ZnO. The phonon band structure of Te-doped sodalite ZnO (panel (b) of figure 3) is clearly shifted toward lower energies, due to the large atomic mass of Te. Except for that, phonon bands are similar to those of undoped sodalite (panel (a) of figure 3). This similarity is not surprising since Te induces an isotropic deformation, preserving the symmetry of the structure. Te phonon modes are located at around 45 cm^{-1} and the low energy phonon DOS is dominated by phonons from both Zn and the dopant atoms. For Br-doped sodalite, dopants and zinc phonon modes are at higher energies, in the range from around 75 cm^{-1} (panel (c) of figure 3). This situation is similar to I-doped sodalite ZnO (see supplementary material). By contrast, doping with F (panel (d) of figure 3) leads to a quite different phonon band structure, as in this case the deformation of the structure is strong and anisotropic with dopant modes located at higher energies between 160 and 230 cm^{-1}.

3.4. Superconducting properties

In order to investigate the superconducting properties of degenerate sodalite ZnO, we used the McMillan formula for the superconducting transition temperature [52, 53].

$$T_c = \frac{\omega_{\log}}{1.2} \exp\left[-\frac{1.04(1+\lambda)}{\lambda - \mu^\star(1+0.62\lambda)}\right], \tag{1}$$

where ω_{log} is a weighted average of phonon frequencies, and

$$\lambda = 2\int \frac{\alpha F^2(\omega)}{\omega} d\omega \tag{2}$$

is an average of the electron–phonon interaction. These quantities are calculated from the Eliashberg spectral function $\alpha^2F(\omega)$. The effective Coulomb interaction was mimiced by the phenomenological $\mu^\star = 0.1$. The right panels of figure 3 present the Eliashberg spectral functions $\alpha^2F(\omega)$ calculated for doped sodalite ZnO. In case of doping by Te (panel (b) of figure 3), the coupling between electrons and phonons is particularly efficient at low frequencies, where Te and Zn low-energy modes are particularly effective to increase λ (see equation (2)). Indeed, the integrated λ plotted in figure 3 (right panels) shows a fast increase at low frequencies. The calculated T_c for Te-doped sodalite is 7 K. By increasing $\mu^\star$ to 0.13, T_c decreases to 6 K. These temperatures are quite close to the T_c measured for Ba-doped silicon clathrates [20], and are consistent with the transition temperatures of doped group-IV semiconductors. This shows that superconductivity is certainly possible in doped ionic materials.

Superconducting T_c, λ, and ω_{log} for different compounds are summarized in table 2. The doping concentration has a major influence on the electronic DOS at the Fermi level and therefore on the superconducting properties. For instance, the critical temperature increases for Te from 2 K, when every other cage is filled and to 7 K when all cages are filled. The transition temperature tends to increase with the atomic mass of the dopant, similar to what occurs in doped silicon clathrates.

These results raise questions about the main mechanism responsible for the superconductive properties in ZnO sodalite. On one hand, the projection of the electron-phonon coupling onto the electronic states shows that the contribution of the dopant atom is substantial when T_c is larger (see figure 2). Indeed, a sizable T_c is observed only for the case of Te and I doping, where there is a strong hybridization of dopant and O states at the Fermi level (see figure 2 and supplementary material). The total coupling is reduced for Cl and Br doping, where the hybridization is smaller, and it gets even smaller in the case of F doping, where the hybridization is absent. This hybridization appears important to explain the observed differences between F-, Cl-, Br-, and Te-doped sodalite. However, the hybridization alone cannot explain the different T_c obtained for Te- and I-doped sodalite. Moreover, the DOS at the Fermi energy $N(E_F)$ is not directly correlated with the electron–phonon coupling λ since Te-doped sodalite possesses the best superconductive properties with a lower DOS at the Fermi energy (see

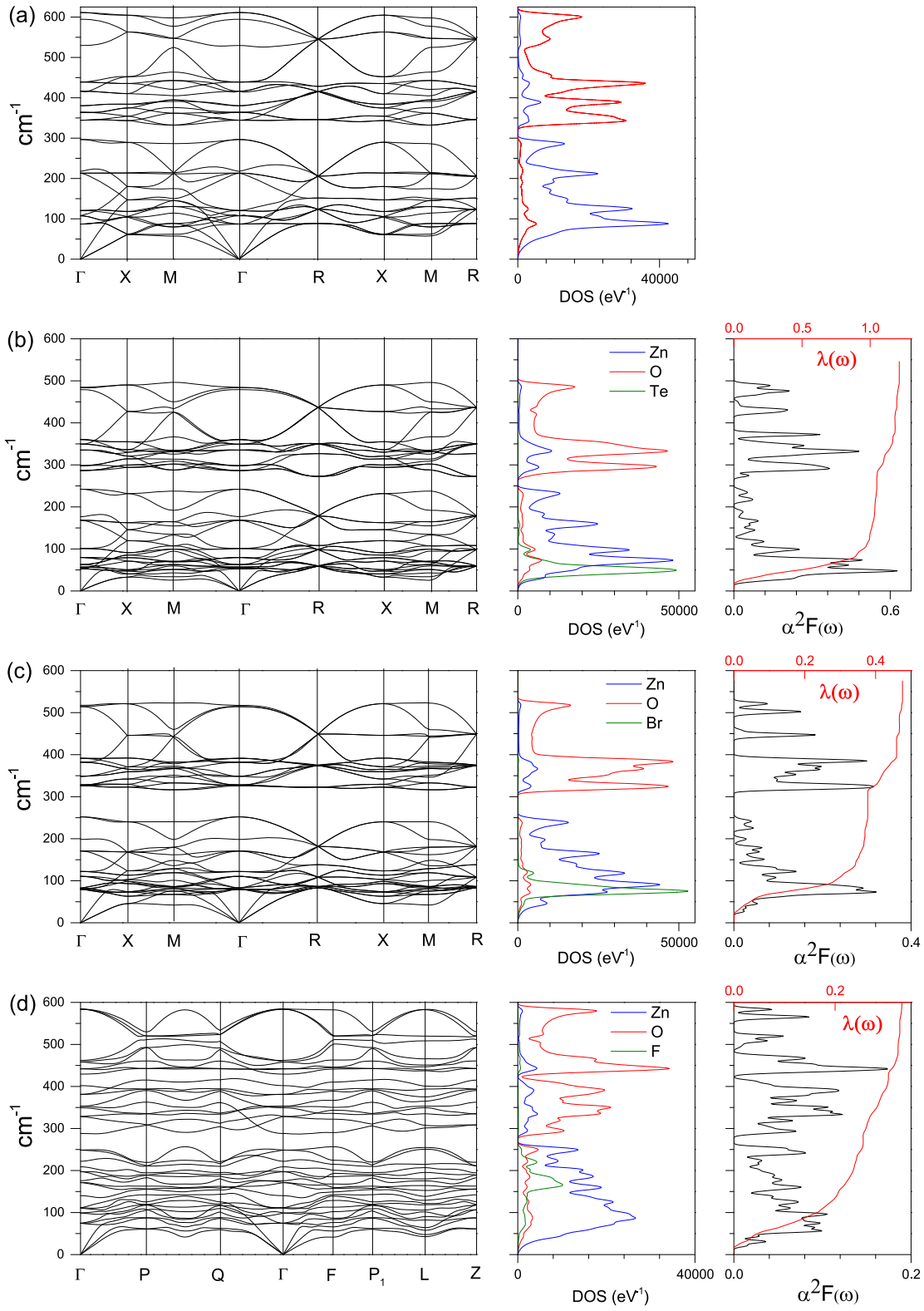

Figure 3. Phonon band structures (left), decomposition of the phonon DOS on each element (middle), and associated Eliashberg functions together with integrated λ (right) for (b) Te-, (c) Br-, and (d) F-doped sodalite ZnO. The phonon band structure of undoped sodalite ZnO is depicted in panel (a) with the associated DOS.

table 1). Clearly, considerations on the electronic states alone are not sufficient to explain the origin of superconductivity in sodalite ZnO.

On the other hand, the phonon projected DOS shows that both dopant and zinc atoms induce low frequency modes (see figure 3 and supplementary material). Clearly, the heavier the dopant, the lower the frequencies of the dopant phonon modes. I-, Br-, and Cl-doped sodalite have similar phonon DOS at low frequencies, with the

Table 2. Superconducting properties T_c (in K), λ (dimensionless) and ω_{log} (in K) for different degenerate doped sodalite and for two dopant concentrations (8% and 14%).

	8%			14%		
	T_c	λ	ω_{log}	T_c	λ	ω_{log}
Te	2.5 K	0.58	124 K	7.0 K	1.20	98 K
I	0.8 K	0.40	187 K	2.0 K	0.50	163 K
Br	0.3 K	0.35	179 K	1.6 K	0.48	158 K
Cl	0.2 K	0.34	168 K	1.6 K	0.49	144 K
F	0.2 K	0.33	160 K	—	—	—

lowest intense peak located around 75 cm^{-1} and ω_{log} around 150 K. These systems have similar phonon DOS, similar Eliashberg functions, different electronic DOS at the Fermi level but similar superconductive properties. Te-doped sodalite shows the lowest and more important phonon modes (last peak at around 45 cm^{-1}, ω_{log} = 98 K) and displays the highest T_c, while F-doped sodalite has the lowest T_c together with a weak low-frequency phonon DOS. Furthermore, we observe that the phonon modes induced by zinc atoms at low frequencies are also strongly dependent on the nature of the dopant, as illustrated in figure 3 and in the supplementary material. For instance, I- and Cl-doped sodalite have similar superconductive properties, but the low frequency modes from Cl are less pronounced and located at a higher energy than phonon modes from I. Since ω_{log} are similar for these two structures, this weakness is therefore compensated by the fact that the Zn phonon modes are more important at low frequencies in the case of Cl-doped sodalite. Thus, the presence of Zn and dopant phonon modes at low frequencies is very important to increase λ. All in all, these observations indicate that, first, a substantial hybridization of dopant and O states at the Fermi level is necessary but not sufficient to get higher superconducting critical temperatures T_c. Then, the low energy phonons due to Zn and dopant atoms are mainly responsible for the increase of electron-phonon coupling λ in doped ZnO sodalite.

The appearance of conventional superconductivity in a iono-covalent compound is original, but that situation raises questions about the role of ionicity. The decomposition of the electron–phonon coupling onto the phonon DOS (see figure 3) illustrates the critical contribution of low energy phonon modes (related to both dopants and Zn atoms). Concerning the electronic DOS, a substantial hybridization of dopant states with oxygen states at the Fermi level turns out to be necessary to obtain a higher T_c. In fact, given that the dopants are p-type, the hybridization is favored by the ionicity of the Zn-O bond, as it induces a negative charge on oxygen atoms. Therefore, the ionic character of ZnO has an important role in the appearance of a superconductive state in the p-doped sodalite structure. This is an original situation coming from the very ionic nature of ZnO.

4. Conclusion

In conclusion, we predicted from *ab initio* calculations the emergence of superconductivity in a ionic and large band gap semiconductor, sodalite ZnO. As a consequence of strong doping, this material is a degenerate semiconductor, which becomes a superconductor with calculated critical temperatures of up to 7 K. The highest transition temperature is obtained for doping with an heavy element like tellurium, a situation similar to the one known for silicon clathrates. We point out that the superconductivity in ZnO sodalite relies on a strong hybridization of the electronic states of oxygen and dopant atoms.

Moreover, dopants with a high atomic mass are more suitable for superconductivity in this class of materials due to the greater electron–phonon coupling, and the weak and isotropic deformation of the structure. We found that the key to superconductivity is to achieve high-enough doping without substantially deforming the starting structure, as the iono-covalent bonding leads to electron–phonon coupling capable of producing superconductivity.

This work also highlights the critical importance of the interplay of two phenomena to enhance the superconductive transition temperature: (i) the presence of low- frequency phonons associated with vibrations of either dopant or zinc atoms and (ii) a substantial hybridization between oxygen and dopant electronic levels at the Fermi level with an important proportion of dopant electronic states.

We believe that our results are generalizable and that superconductivity can be found not only in other cage-like structures of III-V or II-VI semiconductors, but also in more standard wurtzite and zincblende structures, provided that a convenient doping procedure can be found.

Acknowledgments

MALM and SB acknowledge financial support from the French ANR projects ANR-08-CEXC8–008-01 and ANR-12-BS04-0001-02. Computational resources were provided by GENCI (project x2012096017). J A Flores-Livas acknowledges financial support from EUs 7th Framework Marie-Curie Scholarship Program within the 'ExMaMa' Project (329386).

References

[1] Ekimov E A, Sidorov V A, Bauer E D, Mel'nik N N, Curro N J, Thompson J D and Stishov S M 2004 *Nature* **428** 542–5
[2] Bustarret E *et al* 2006 *Nature* **444** 465–8
[3] Herrmannsdörfer T *et al* 2009 *Phys. Rev. Lett.* **102** 217003
[4] Kriener M, Muranaka T, Kato J, Ren Z A, Akimitsu J and Maeno Y 2008 *Sci. Technol. Adv. Mater.* **9** 044205
[5] Muranaka T, Kikuchi Y, Yoshizawa T, Shirakawa N and Akimitsu J 2008 *Sci. Technol. Adv. Mater.* **9** 044204
[6] Crespi V H 2003 *Nat. Mater.* **2** 650–1
[7] Bednorz J G and Müller K A 1986 *Z. Phys. B: Condens. Matter* **64** 189–93
[8] Nagamatsu J, Muranaka T, Zenitani Y and Akimitsu J 2001 *Nature* **410** 63–4
[9] Buzea C and Yamashita T 2001 *Supercond. Sci. Technol.* **14** R115
[10] Gunnarsson O 1997 *Rev. Mod. Phys.* **69** 575–606
[11] Flores-Livas J A, Debord R, Botti S, San Miguel A, Marques M A L and Pailhès S 2011 *Phys. Rev. Lett.* **106** 087002
[12] Flores-Livas J A, Debord R, Botti S, San Miguel A, Pailhès S and Marques M A L 2011 *Phys. Rev.* B **84** 184503
[13] Weller T E, Ellerby M, Saxena S S, Smith R P and Skipper N T 2005 *Nat. Phys.* 1 **1**
[14] Kim J S, Boeri L, O'Brien J R, Razavi F S and Kremer R K 2007 *Phys. Rev. Lett.* **99** 027001
[15] Minami T 2005 *Semicond. Sci. Technol.* **20** S35
[16] Guo H, Lin Z, Feng Z, Lin L and Zhou J 2009 *J. Phys. Chem.* C **113** 12546–50
[17] Hapiuk D, Masenelli B, Masenelli-Varlot K, Tainoff D, Boisron O, Albin C and Mélinon P 2013 *J. Phys. Chem.* C **117** 1932–7447
[18] Pacholski C, Kornowski A and Weller H 2002 *Angew. Chem., Int. Ed.* **41** 11521–3773
[19] Özgür U, Alivov Y I, Liu C, Teke A, Reshchikov M A, Doğan S, Avrutin V, Cho S J and Morkoç H 2005 *J. Appl. Phys.* **98** 041301
[20] Connétable D *et al* 2003 *Phys. Rev. Lett.* **91** 247001
[21] Tournus F, Masenelli B, Mélinon P, Connétable D, Blase X, Flank A M, Lagarde P, Cros C and Pouchard M 2004 *Phys. Rev.* B **69** 035208
[22] Blase X, Bustarret E, Chapelier C, Klein T and Marcena C 2009 *Nature Mater* **8** 375–82
[23] Kulkarni A J, Zhou M, Sarasamak K and Limpijumnong S 2006 *Phys. Rev. Lett.* **97** 105502
[24] Carrasco J, Illas F and Bromley S T 2007 *Phys. Rev. Lett.* **99** 235502
[25] Morgan B J 2009 *Phys. Rev.* B **80** 174105
[26] Zwijnenburg M A, Illas F and Bromley S T 2010 *Phys. Rev. Lett.* **104** 175503
[27] Zhang S, Zhang Y, Huang S, Wang P and Tian H 2013 *Chem. Phys. Lett.* **557** 102–5
[28] Wang B, Wang X and Zhao J 2010 *J. Phys. Chem.* C **114** 5741–4
[29] Liu Z, Wang X, Cai J, Liu G, Zhou P, Wang K and Zhu H 2013 *J. Phys. Chem.* C **117** 17633–43
[30] Baei M T, Peyghan A A and Bagheri Z 2013 *C. R. Chim.* **16** 122–8
[31] Dmytruk A, Dmitruk I, Blonskyy I, Belosludov R, Kawazoe Y and Kasuya A 2009 *Microelectron. J.* **40** 218–20
[32] Heinzelmann J, Koop A, Proch S, Ganteför G F, Łazarski R and Sierka M 2014 *J. Phys. Chem. Lett.* **5** 2642–8
[33] Bulgakov A V, Ozerov I and Marine W 2003 arXiv:physics/0311117
[34] Liu Z, Wang X, Liu G, Zhou P, Sui J, Wang X, Zhu H and Hou Z 2013 *Phys. Chem. Chem. Phys.* **15** 8186–98
[35] Hapiuk D, Marques M A L, Melinon P, Flores-Livas J A, Botti S and Masenelli B 2012 *Phys. Rev. Lett.* **108** 115903
[36] Agrawal R, Peng B and Espinosa H D 2009 *Nano Lett.* **9** 4177–83
[37] He M R, Yu R and Zhu J 2012 *Angewandte Chemie Int. Edition* **51** 7744–7
[38] Freysoldt C, Grabowski B, Hickel T, Neugebauer J, Kresse G, Janotti A and van de Walle C G 2014 *Rev. Mod. Phys.* **86** 253–305
[39] Cros C and Pouchard M 2009 *C. R. Chim.* **12** 1014–56
[40] Melinon P and Masenelli B (ed) 2012 *From Small Fullerenes to Superlattices: Science and Applications* 1st ed (Singapore; London: Pan Stanford)
[41] Frank F C and Kasper J S 1958 *Acta Crystallogr.* **11** 184–90
[42] Kasper J S, Hagenmuller P, Pouchard M and Cros C 1965 *Science* **150** 1713–4
[43] Phillips J C 1973 *Bonds and bands in semiconductors* (New York: Academic)
[44] Gonze X *et al* 2005 *Z. Kristallogr.* **220** 558
[45] Gonze X *et al* 2009 *Comput. Phys. Commun.* **180** 2582 –15
[46] Perdew J P, Burke K and Ernzerhof M 1996 *Phys. Rev. Lett.* **77** 3865–8
[47] Fuchs M and Scheffler M 1999 *Comput. Phys. Commun.* **119** 67–98
[48] Monkhorst H J and Pack J D 1976 *Phys. Rev.* B **13** 5188–92
[49] Savrasov S Y and Savrasov D Y 1996 *Phys. Rev.* B **54** 16487–501
[50] Savrasov S Y 1996 *Phys. Rev.* B **54** 16470–86
[51] Baroni S, de Gironcoli S, Dal Corso A and Giannozzi P 2001 *Rev. Mod. Phys.* **73** 515–62
[52] McMillan W L 1968 *Phys. Rev.* **167** 331–44
[53] Allen P B and Dynes R C 1975 *Phys. Rev.* B **12** 905–22
[54] Blase X 2011 *C. R. Phys.* **12** 584–90